Coherent control in semiconductor quantum dots: Reduced optical gain thresholds via biexciton control

David Gerbasi,* Gregory D. Scholes, and Paul Brumer
Department of Chemistry, Center for Quantum Information and Quantum Control, Institute for Optical Sciences, University of Toronto, 80 St. George Street, Toronto, Canada M5S 3H6

(Received 11 March 2010; revised manuscript received 22 July 2010; published 21 September 2010)

Coherent control theory is used to show that one can manipulate biexciton vs exciton populations in semiconductor quantum dots (QDs) in a typical dissipative environment. Both aligned and randomly oriented quantum dots are considered, and population control is shown to be considerable. An application to CdSe QD shows that the proposed coherent control scenario results in a significant reduction in pump intensity for the onset of optical gain.

DOI: 10.1103/PhysRevB.82.125321 PACS number(s): 73.21.La, 78.47.−p

I. INTRODUCTION

Colloidal semiconductor quantum dots (QDs) have been studied extensively in order to elucidate their properties in detail.[1–7] Such investigations have been enabled largely by improvements in sample preparation and hence sample quality. In particular, optical gain has been examined with a view to determining how to fabricate practical quantum dot lasers.[8–13] Quantum dot lasers would be wavelength tunable according to the sample characteristics, which are tuned via confinement. Moreover, their production could be achieved using solution processing methods, and the material itself is photostable relative to organic laser media.

Important fundamental investigations of QD lasers have shown that the gain threshold for CdSe QDs occurs at a pump intensity that ensures an average population of approximately one exciton per QD. However, achieving that exciton population level is limited by biexciton recombination, which is rapid for small quantum dots. Recent work has aimed to eliminate this restriction by tuning the electron-electron interaction in the QDs through the preparation of core-shell heterostructure materials. In this paper we explore the possibility of an alternative approach, based on coherent control.[14–16] Specifically, we show that a carefully designed optical pump can substantially increase biexciton population over that naturally produced by Poisson statistics. Hence biexciton populations can be controlled and the optical gain threshold can be achieved at substantially lower pump intensity.

Control is made possible, as in all other coherent control scenarios, by the introduction of two or more competing optical pathways to the same target state. The resulting interference allows for the constructive or destructive manipulation of probability amplitudes and control is attained by varying the relative phase and amplitude between the two pathways.[14] In this QD case we custom tailor a two-photon vs two-photon interference scenario,[17,18] shown below to be highly effective.

QD spectroscopy is described in terms of single-excitation configurations whereby an electron is promoted from the fourfold-degenerate valence band to the doubly degenerate conduction band.[19–21] Those configurations are mixed by the exchange interaction, leading to an exciton fine structure.[21–26] Evidence for the existence of the exciton fine structure comes from careful photoluminescence studies of ensembles and single QDs (Refs. 27–31) as well as certain nonlinear optical experiments.[32] An important characteristic of the QD exciton fine structure is that it represents a manifold of spectroscopic states.[33,34] Each bright state may each be optically excited according to selection rules for absorption of either circularly or linearly polarized light. Consequently, there are various kinds of biexcitons that are prepared by optical excitation of two excitons. Such biexcitons are known to recombine to excitons on a time scale of tens of picosecond, depending on the size of the CdSe QD. It is shown in the present work how interference between pathways for preparing a biexciton by sequential excitation of two excitons can be incorporated in a coherent control scenario that allows one to enhance or suppress biexciton formation relative to exciton formation. This is possible despite the complex fine-structure manifold, the inhomogeneous spectral broadening, and the random orientation of each QD in the ensemble relative to the laboratory frame. Other than the evident interest in controlling the biexciton population, this approach offers an opportunity for low threshold quantum dot gain media.

The paper is organized as follows. Section II reviews the selection rules associated with quantum dot optical transitions and the effects of angular averaging are described. Section III outlines the coherent control scenario used to control the level populations of the quantum dot. In this approach we make use of interfering pathways in the presence of a background with the overall system dynamics described by the system density matrix. In Sec. IV, control results are shown for both aligned and isotropic systems. Lastly, Sec. V provides a brief summary and conclusion.

II. SELECTION RULES

The probability amplitude of optical transitions in a QD is determined by the matrix element of the dipole operator between the hole wave functions $|J,M\rangle$ and the electron wave functions $|J',M'\rangle$, where J and J' are the total angular momentum quantum numbers for the hole and electron wave functions, respectively, and M and M' are their corresponding Z projections.[19–21] In order to maintain a relatively simple, yet precise, control scheme, we consider here only the interband transitions to and from the lowest quantum

level of electrons caused by the absorption and emission of linear or circular polarized light. Therefore, the relevant quantum numbers are $J'=1/2$ and $J=3/2$ with $M=-J,\ldots,J$.[19]

The appropriate matrix elements are evaluated by expressing each hole wave function as an angular wave function $Y_{J,M}(\phi,\theta)$ and, similarly, each electron wave function as $Y_{J',M'}(\phi,\theta)$. In the electron-hole representation, the probability amplitude of an optical transition is then proportional to

$$A \propto \langle J',M'|\epsilon\cdot\vec{\mu}|J,M\rangle. \tag{1}$$

Making use of the following relations:[35]

$$Y_{J,M}(\phi,\theta) \equiv (-1)^M\left(\frac{2J+1}{4\pi}\right)^{1/2} D^J_{M,0}(\phi,\theta,\chi) \tag{2}$$

and

$$\mu_l \equiv \epsilon\cdot\vec{\mu}_l = f_l t_{q_l}\sum_{K=-1}^{K=1}\mu_l^{(K)}\{D^1_{K,q_l}(\phi,\theta,\chi)+p_l(-1)^{q_l}D^1_{K,-q_l}(\phi,\theta,\chi)\}, \tag{3}$$

where

$$\mu_l^{(0)} \equiv \mu_l^z, \quad \mu_l^{(-1)} \equiv (\mu_l^x - i\mu_l^y)/\sqrt{2}, \quad \mu_l^{(1)} \equiv -(\mu_l^x + i\mu_l^y)/\sqrt{2}, \tag{4}$$

and $t_0=1/2$ and $t_1=1/\sqrt{2}$ with $f_l=1$, $q_l=0$, and $p_l=1$ for $\hat{\epsilon}_l$ along the Z axis, $f_l=-1$, $q_l=1$, and $p_l=1$ for $\hat{\epsilon}_l$ along the X axis, and $f_l=i$, $q_l=1$, and $p_l=-1$ for $\hat{\epsilon}_l$ along the Y axis, Eq. (1) can be rewritten as

$$A \propto (-1)^{M+M'}\left(\frac{2J'+1}{4\pi}\right)^{1/2}\left(\frac{2J+1}{4\pi}\right)^{1/2} \times\sum_{k=-1}^{1}\mu_k\langle D^{J'}_{M',0}|D^1_{k,0}|D^J_{M,0}\rangle. \tag{5}$$

Here $D^J_{M,K}$ are the rotational matrices in Edmonds notation.[36] A general expression for the angular integral in the above equation is obtained in terms of 3-j symbols as,[36]

$$A \propto (-1)^M(2J'+1)(2J+1)\sum_{k=-1}^{1}\mu_k\begin{pmatrix} J' & 1 & J \\ -M' & k & M\end{pmatrix} \times\begin{pmatrix} J' & 1 & J \\ 0 & 0 & 0\end{pmatrix}. \tag{6}$$

The selection rule $\Delta J=\pm 1$ is a consequence of the second 3-j symbol in Eq. (6); the first 3-j symbol gives the selection rules for M. Here the value of k can either be $0,\pm 1$, where $k=0$ corresponds to linear Z polarization and $k=\pm 1$ corresponds to right and left circular polarizations. For $k=0$, $M=M'$ and $\Delta M=0$. For $k=\pm 1$, $M=M'\pm 1$ and $\Delta M=\pm 1$. Taking into account only the transitions from the electrons S states, Z polarized light excites from the electron state $|1/2,1/2\rangle$ to the hole state $|3/2,1/2\rangle$, right circular polarization excites the transitions between electron state $|1/2,-1/2\rangle$ and hole state $|3/2,-3/2\rangle$ and electron state $|1/2,1/2\rangle$ and hole state $|3/2,-1/2\rangle$, left circular polarization excites the transitions between electron state $|1/2,1/2\rangle$ and hole state $|3/2,3/2\rangle$ and electron state $|1/2,-1/2\rangle$ and hole state $|3/2,1/2\rangle$. Note that these results are in accord with previous studies.[19]

Consider now the case of rotational averaging where $M\rightarrow -M$. For Z polarization[36]

$$\begin{pmatrix} J' & 1 & J \\ -M & 0 & M\end{pmatrix}\xrightarrow[M\rightarrow -M]{}(-1)^{J'+J+1}\begin{pmatrix} J' & 1 & J \\ -M & 0 & M\end{pmatrix}. \tag{7}$$

Angular averaging introduces an additional phase factor $(-1)^{J'+J+1}$ that needs to be taken into consideration when constructing the coherent control scenario. Our computations show that it has no effect on the control. However, for the case of right circular polarized light, under rotational averaging,

$$\begin{pmatrix} J' & 1 & J \\ -(M+1) & 1 & M\end{pmatrix}\xrightarrow[M\rightarrow -M]{}(-1)^{J'+J+1}\begin{pmatrix} J' & 1 & J \\ -(M-1) & -1 & M\end{pmatrix} \tag{8}$$

and, similarly, for left circularly polarized light

$$\begin{pmatrix} J' & 1 & J \\ -(M-1) & -1 & M\end{pmatrix}\xrightarrow[M\rightarrow -M]{}(-1)^{J'+J+1}\begin{pmatrix} J' & 1 & J \\ -(M+1) & 1 & M\end{pmatrix}. \tag{9}$$

That is, Eqs. (8) and (9) show that angular averaging changes right circular polarization into left circular polarization and vice versa. Therefore, the control scenario must not explicitly depend on only either right or left circular polarization but rather have the same dependence on both.

III. CONTROL SCENARIO

Consider a quantum dot, specifically a CdSe QD whose electronic energy levels are given in Ref. 24, with a crystal axis aligned along the Z laser polarization axis. The more

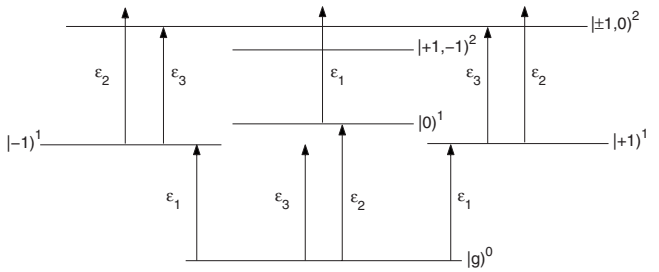

FIG. 1. Control scenario as described in text for an isotropic system.

general case of an isotropic system is considered below and includes angular averaging over all possible solid angles. As shown in Fig. 1, control arises by operating on the system with two Z polarized lasers of different frequency and one laser that is either left or right circularly polarized. Various laser attributes such as amplitudes, detunings, etc., can be varied to optimize specific control targets, as discussed later below. In all cases one Z polarized laser (denoted ε_2) is tuned to excite the ground state $|g)^0$ to the exciton state $|0)^1$ (ΔE=2.202 eV) while the second Z polarized laser (denoted ϵ_3) is tuned to excite the exciton state $|\pm1)^1$ to the biexciton state $|\pm1,0)^2$ (ΔE=2.158 eV). The biexciton splitting (between the two $|\pm1,0)^2$ states) is 18 meV. The circularly polarized laser (denoted ε_1) excites the ground state $|g)^0$ to the exciton state $|\pm1)^1$ (ΔE=2.154 eV) and the exciton state $|0)^1$ to the biexciton state $|\pm1,0)^2$ (ΔE=2.110 eV) (see Fig. 1). The general notation used here is $|\Delta M,\ldots,\Delta M')^N$, where N indicates the number of electrons excited and ΔM is the change in the M quantum number of each excited electron as predicted by the selection rules. For example, $|+1,-1)^2$ is a biexciton state reached using both right and left circular polarizations.

Control in this scenario arises from the existence of two competing pathways to the biexciton state $|\pm1,0)^2$: $|g)^0 \rightarrow |0)^1 \rightarrow |\pm1,0)^2$ via excitation by ϵ_2 and ϵ_1, and $|g)^0 \rightarrow |\pm1)^1 \rightarrow |\pm1,0)^2$ due to excitation by ϵ_1 and ϵ_3. The choice of ±1 depends on the either using right or left circular polarization but the overall scenario is not affected by the angular averaging since there is no preference for either left or right circularly polarized light in this scenario. Hence, by varying the relative phase between the two Z polarized lasers, it is possible to control the biexciton population. The additional state $|+1,-1)$ populated by $2\epsilon_1$ excitation does not participate in any control route. Hence, the inadvertent participation of this state serves to diminish control.

The assumption that the crystal axis is aligned along the Z laser polarization is valid only for aligned systems. In an isotropic system, it is necessary to consider an ensemble wherein the crystal axis system of each QD constituent may be aligned along any possible direction. This is easily accomplished by averaging over all possible solid angles (see Ref. 21).

Essentially, the result is that the system has an equal number of quantum dots whose crystal axis is, on average, aligned along either X, Y, or Z. As such, consider the case were the crystal axis is aligned along the X space axis. The crystal will "see" the two originally polarized Z lasers as being polarized along the Y axis and the circularly polarized light will be viewed as having a Z component and an X component that are out of phase by $\pi/2$. As such, the crystal is affected by two lasers of Y polarization, one of Z polarization and one of X polarization that is out of phase by $\pi/2$ relative to the Z laser. Similarly, for the case where the crystal axis is aligned along the Y space axis, the crystal will be operated on by two lasers of X polarization, one of Y polarization and one of Z polarization that is out of phase by $\pi/2$ relative to the Y laser. There is then a total of seven quantum dot states that take part in the control scheme: the ground state $|g)^0 \equiv |1\rangle$, three exciton states $|1)^1 \equiv |2\rangle$, $|-1)^1 \equiv |3\rangle$, and $|0)^1 \equiv |4\rangle$, and three biexciton states $|+1,-1)^2 \equiv |5\rangle$, $|1,0)^2 \equiv |6\rangle$, and $|-1,0)^2 \equiv |7\rangle$. Relabeling the quantum dots states in this manner is done for notational convenience below.

The dynamics of the isolated QD system in the presence of radiation is described by the time-dependent Schrödinger equation

$$i\hbar\, \partial|\Psi\rangle/\partial t = H_{tot}(t)|\Psi\rangle \tag{10}$$

with

$$H_{tot}(t) = H_Q - \sum_k \vec{\mu}_k \cdot \mathbf{E}_k(t), \tag{11}$$

where H_Q is the quantum dot Hamiltonian, $\vec{\mu}_k$ is the electric transition dipole moment, and $\mathbf{E}_k(t)$ is the electric field. Expanding $|\Psi\rangle$ in eigenstates $|j\rangle$ of the quantum dot (i.e., $H_Q|j\rangle = E_j|j\rangle$) as

$$|\Psi\rangle = \sum_{j=1}^{7} b_j(t)\exp(-iE_jt/\hbar)|j\rangle \tag{12}$$

and substituting Eq. (12) into Eq. (10), gives a set of seven coupled differential equations.

The overall dynamics of the system within an environment, however, requires a density-matrix picture. Here we adopt a rudimentary model of the system density matrix ρ in the presence of a dissipative bath and in the presence of an electric field[35] as

$$\dot{\rho} = -\frac{i}{\hbar}[H_{tot},\rho] + \hat{A} + \hat{B} + \hat{C}, \tag{13}$$

where H_{tot} is given by Eq. (11). The first term on the right-hand side of Eq. (13) describes the system dynamics in the absence of decoherence while the other terms incorporate the system-bath interactions responsible for decoherence and decay. Specifically, the operators $\hat{A}$ and $\hat{B}$, modeled below, represent decay from the biexciton levels and exciton levels, respectively, with decay rates γ_{bi} and γ_{ex}. The operator $\hat{C}$, provided below, describes the overall dephasing rate.

Within this phenomenological model the klth matrix element of Eq. (13) is given by[35]

$$\dot{\rho_{kl}} \equiv \langle k|\dot{\rho}|l\rangle = -\frac{i}{\hbar}\langle k|[H_{tot},\rho]|l\rangle + \langle k|\hat{A}|l\rangle + \langle k|\hat{B}|l\rangle + \langle k|\hat{C}|l\rangle, \tag{14}$$

where the klth matrix elements for the biexciton decay, with rate γ_{bi}, are given by

$$A_{kl} = -\frac{\gamma_{bi}}{2}\rho_{kl},$$

$$A_{kk} = -\gamma_{bi}\rho_{kk},$$

$$A_{ii} = \frac{1}{3}\sum_{k}\gamma_{bi}\rho_{kk}, \tag{15}$$

where the states $|k\rangle$ and $|l\rangle$ are the biexciton levels and states $|i\rangle$ are the exciton levels. Similarly, the klth matrix elements for exciton decay with rate γ_{ex} have the form

$$B_{kl} = -\frac{\gamma_{ex}}{2}\rho_{kl},$$

$$B_{kk} = -\gamma_{ex}\rho_{kk},$$

$$B_{gg} = \gamma_{ex}\rho_{kk} \tag{16}$$

with $|k\rangle$ and $|l\rangle$ now representing the exciton levels and state $|g\rangle$ the ground state. The dephasing contribution with rate γ_{de} is given by

$$C_{ij} = -\frac{\gamma_{de}}{2}\rho_{ij},$$

$$C_{ii} = 0, \tag{17}$$

where $|i\rangle, |j\rangle$ are all participating quantum dot levels.

The integration of the resultant equations is carried out in a straightforward way. Below, algorithms are introduced to seek optimal solutions as a function of laser parameters. We note that the initial and final times for the numerical integration of these equations are chosen as minus and plus six times, respectively, the largest of the optimized laser-pulse widths.

IV. RESULTS

Quantitative results are obtained by numerically solving for the density matrix using Gaussian pulses of the form $\epsilon_i(t) = \beta_i \exp\{-[(t_i - t)]/\alpha_i]^2\}$, where β_i is the field amplitude, t_i is the center of the pulse, and α_i is the pulse width. The transition dipole moments used have a value of 2 D.[37] The decay time $(1/\gamma_{bi})$ from the biexciton levels is set to 40 ps while that $[(1/\gamma_{ex})]$ from the exciton levels is 20 ns. The fastest decoherence time $(1/\gamma_{de})$, the dephasing time, is set to 500 fs. Note that by using short pulses on the order of femtosecond both the biexciton and exciton decay processes do not play a significant role in the control dynamics. Also note that specific quantum dot parameters used are those of the CdSe quantum dot but that the overall scheme should be transferable to any quantum dot with similar energy-level structure.

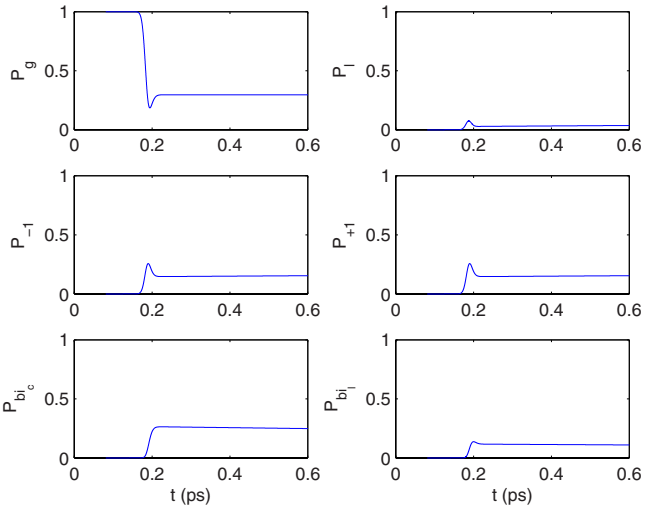

FIG. 2. (Color online) Population of each quantum dot energy level as a function of time for an isotropic system. Here, only one right circularly polarized laser pulse operates on the system where $\beta_1 = 9.997 \times 10^{-4}$ a.u. $(3.516 \times 10^{10}$ W/cm$^2)$, $\alpha_1 = 17.7$ fs, $t_1 = 0.187$ ps, and the laser is detuned by $\Delta = -29.9$ cm^{-1} from the transition between $|g)^0$ and $|\pm 1)^1$. Here P_g corresponds to the ground-state population, P_l the exciton state $|0)^1$, P_{-1} the exciton state $|-1)^1$, P_{+1} the exciton state $|+1)^1$, P_{bi_c} the biexciton state $|+1,-1)^2$, and P_{bi_l} the sum of the biexciton states $|\pm 1,0)^2$. Peak powers are indicated in parentheses.

For comparison purposes below it is of interest to first examine a simple excitation picture. Consider, for example, an isotropic medium where the system is under the influence of only one laser (either linear or circular polarization), which should excite all exciton and biexciton levels. For example, if only the right circularly polarized laser is incident on the system, then upon angular averaging the system should effectively see both right and left circularly polarized light, as well as linearly polarized light along the Z axis. Hence, there should also be no bias toward either of the exciton levels $|+1)^1$ and $|-1)^1$ or biexciton levels $|+1,0)^2$ and $|-1,0)^2$. Figure 2, whose figure caption contains the laser parameters, confirms these expectations. Here the biexciton population has been optimized using simulated annealing.[38] In particular, the system was optimized to enhance the total biexciton population, i.e., the sum of all three biexciton levels $|+1,0)^2$, $|-1,0)^2$, and $|+1,-1)^2$, resulting in a biexciton population of 35.6%

Consider then the results of the control scenario in an oriented system such as the experimentally feasible oriented nanorods. (For example, Alivisatos and co-workers[39] have demonstrated that CdSe nanorods align into a nematic liquid crystalline phase.) As shown in Fig. 3, by considering a fixed system of quantum dots whose crystal axis is aligned along the Z polarization axis, population control is significant. That is, the biexciton population can be varied from 1.86% to 84.6% by simply changing the relative phase between the two Z polarized lasers.

Control becomes less efficient in an isotropic system due to angular averaging. To obtain the best possible control in

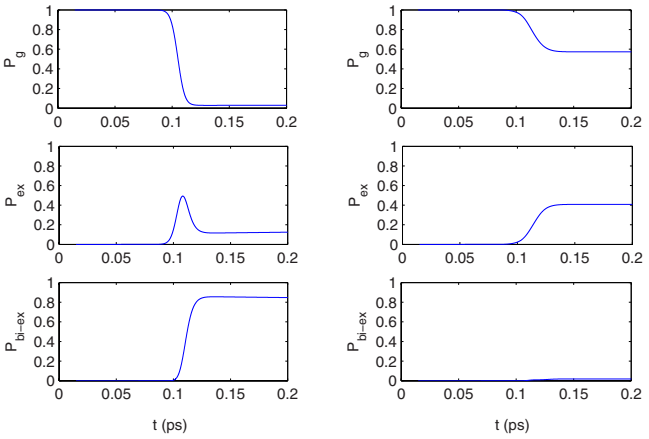

FIG. 3. (Color online) Coherent control of an aligned quantum dot system. The left column corresponds to the enhancement of biexciton and the right column corresponds to the suppression of biexciton. Note that the difference between the enhancement and the suppression of biexciton is attained by changing the relative phase between the two Z polarized lasers by adding π. Also note that the exciton and biexciton populations are the sum of all three individual exciton and biexciton levels, respectively. The laser parameters are $\beta_1=3.731\times10^{-4}$ a.u. (4.8986×10^9 W/cm^2), $\beta_2=9.9930\times10^{-4}$ a.u. (3.5141×10^{10} W/cm^2), $\beta_3=7.127\times10^{-4}$ a.u. (1.7874×10^{10} W/cm^2), $\alpha_1=15.4$ fs, $\alpha_2=10.5$ fs, $\alpha_3=15.9$ fs, $t_1=108.4$ fs, $t_2=106.9$ fs, and $t_3=110.5$ fs. The laser detunings are $\Delta_1=120.35$ cm^{-1}, $\Delta_2=129.82$ cm^{-1}, and $\Delta_3=108.54$ cm^{-1}.

this system, we varied the laser field strengths between 3.519×10^4 and 3.519×10^{10} W/cm^2, the pulse widths between 10 and 600 fs, the detunings between −150 and 150 cm^{-1}, and the time of the pulses between 30 and 1.8 ps. Optimized results were obtained for this case using simulated annealing.[38] As shown in Fig. 4, significant control over the biexciton population can still be exerted, with the biexciton population varying from 11.3% to 76.1%.

The above control results suggest an additional interesting challenge. Specifically, to what extent can exciton and biexciton population control scenario be used to manipulate the optical gain threshold? The optical gain threshold is achieved when there is an average of one electron-hole pair per quantum dot. Since biexcitons "count twice" toward this goal, and triexcitons are not accessible in CdSe, of interest, is the laser power at which one can increase biexciton formation so as to reduce this threshold. To this end, computations were done on the isotropic system to optimize biexciton populations as a function of the excitation field intensities with all other laser parameters optimized within the limits reported above. Optimization as a function of field intensities is shown in Figs. 5 and 6. In the former only one circularly polarized laser is incident on the system and in the latter the biexciton population is optimized using the control scenario shown in Fig. 1.

In the case of the one laser calculation (Fig. 5), the threshold for population inversion, the point at which the ground-state population density is less than 0.5, occurs at a field intensity of $\approx2.5\times10^8$ W/cm^2. The laser intensity for which the average exciton occupation number per QD is

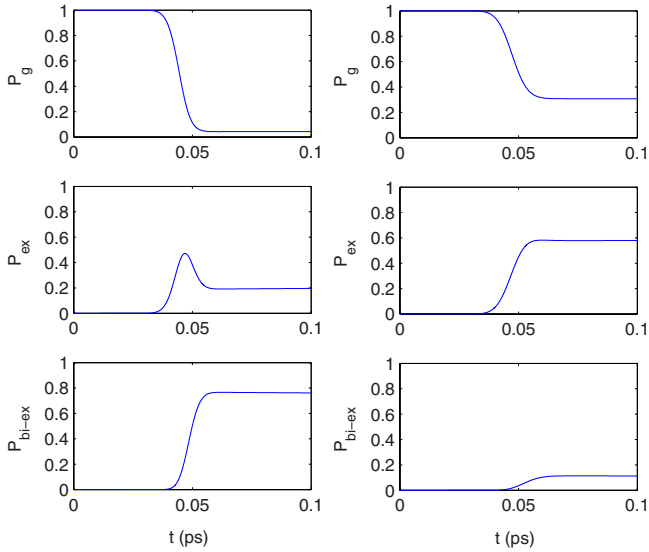

FIG. 4. (Color online) Coherent control of an isotropic quantum dot system. The left column corresponds to the enhancement of biexciton and the right column corresponds to the suppression of biexciton. Note that the difference between the enhancement and the suppression of biexciton is attained by changing the relative phase between the two Z polarized lasers by adding π. Also note that the exciton and biexciton populations are the sum of all three individual exciton and biexciton levels, respectively. The laser parameters are $\beta_1=9.994\times10^{-4}$ a.u. (3.5148×10^{10} W/cm^2), $\beta_2=9.5130\times10^{-4}$ a.u. (3.1846×10^{10} W/cm^2), $\beta_3=9.987\times10^{-4}$ a.u. (3.5097×10^{10} W/cm^2), $\alpha_1=10.1$ fs, $\alpha_2=10.0$ fs, $\alpha_3=10.1$ fs, $t_1=46.9$ fs, $t_2=45.8$ fs, and $t_3=46.5$ fs. The laser detunings are $\Delta_1=44.14$ cm^{-1}, $\Delta_2=24.47$ cm^{-1}, and $\Delta_3=99.39$ cm^{-1}.

unity, offscale in Fig. 5, is at $\approx2.25\times10^{10}$ W/cm^2. Experimentally, this is the intensity at which optical gain is observed. By contrast, when enhanced biexciton formation is targeted in the coherent control scenario (Fig. 6), here with all incident lasers of equal field strength, the threshold for population inversion is found at a field intensity of less than 3.80×10^7 W/cm^2 and the laser intensity for which the average exciton occupation number per QD is unity is $\approx4.25\times10^8$ W/cm^2. (Field parameters at this point are $\alpha_1=210.6$ fs, $\alpha_2=26.73$ fs, $\alpha_3=215.5$ fs, $t_1=576.0$ fs, $t_2=579.4$ fs, $t_3=545.9$ fs, $\Delta_1=-129.905$ cm^{-1}, $\Delta_2=119.762$ cm^{-1}, and $\Delta_3=-4.405$ cm^{-1}.) Hence, the pump intensity for the onset of optical gain in the coherently controlled case is approximately *50 times smaller* than the pump intensity required in the absence of the control scenario.

One can attempt to improve on the goal of reducing the laser intensities needed to achieve optical gain by optimizing[38] system parameters using this explicitly as the sole optimization target. Here, the optimization limits on the parameters are the same as those in Fig. 3 but with an optimization goal of achieving optical gain at lower field intensity implemented by adding a linear penalty associated with the field intensities, i.e., the stronger the field, the greater the penalty. The pulse widths during the optimization were varied between 10 and 3 ps. The results show that the two of the laser intensities needed to achieve optical gain are further reduced compared to those above, and the third is somewhat

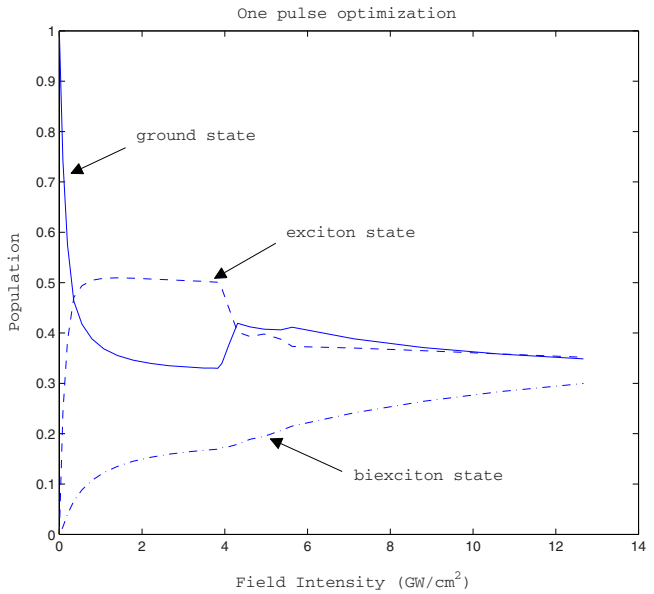

FIG. 5. (Color online) Optimized quantum dot level populations as a function of field intensity. Here only one circular polarized light is applied to excite an isotropic system. Note that the exciton and biexciton populations are the sum of all three individual exciton and biexciton levels, respectively. The abrupt transition near 4×10^9 W/cm^2 is reproducible but cannot be traced to any specific characteristic of the physics. The limits on the optimization parameters are the same as in Fig. 3.

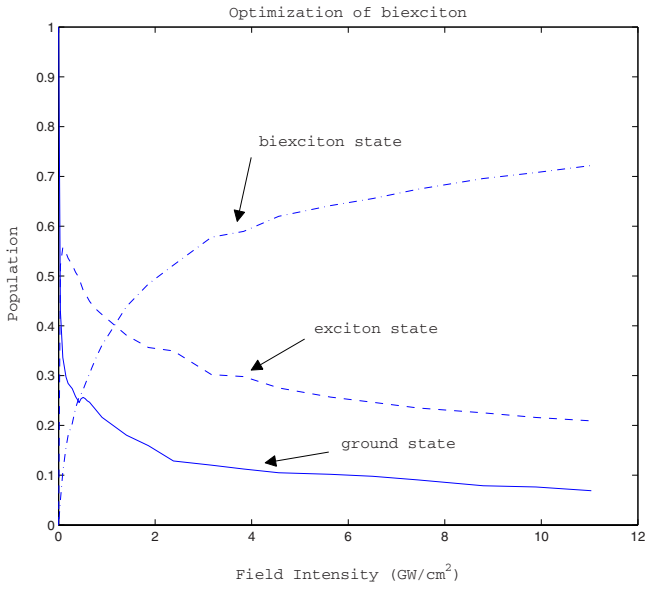

FIG. 6. (Color online) Optimized quantum dot level populations as a function of field intensity. All three laser intensities correspond to those shown on the abcissa and all other parameters were optimized for a given laser intensity. Note that the exciton and biexciton populations are the sum of all three individual exciton and biexciton levels, respectively. The limits on the parameters are the same as in Fig. 3.

increased. Specifically, the optimized parameters are $\beta_1=9.358\times10^{-5}$ a.u. $(3.081\times10^8$ W/cm$^2)$, $\beta_2=9.063\times10^{-5}$ a.u. $(2.891\times10^8$ W/cm$^2)$, $\beta_3=1.829\times10^{-4}$ a.u. $(9.343\times10^8$ W/cm$^2)$, $\alpha_1=656.2$ fs, $\alpha_2=28.54$ fs, $\alpha_3=609.2$ fs, $t_1=21.18$ fs, $t_2=309.0$ fs, $t_3=20.96$ fs, $\Delta_1=-147.11$ cm^{-1}, $\Delta_2=122.61$ cm^{-1}, and $\Delta_3=-40.82$ cm^{-1}. All other optimization limits on the parameters are the same as those in Fig. 3. Also note that the optimized exciton population is 0.606 and the optimized biexciton population is 0.197. Here the biexciton population is, as expected, lower than for the case above where enhanced biexciton population was targeted.

The predicted substantially diminished threshold for optical gain in CdSe QDs is remarkable, a result of the fact that the coherent control scenario can induce a non-Poissonian multiexciton population. For example, the probability that there are k excitons per QD is usually given by

$$P(k)=\frac{N^k\exp(-N)}{k!}, \tag{18}$$

where N is the average number of excitations per complex. This equation determines the exciton to biexciton (to triexciton) ratio obtained in the absence of coherent control and at low enough excitation intensities that the exciton population is not saturated. For example, at an excitation intensity for which there is on average of one exciton per QD, Eq. (18) implies that excitons would be partitioned as 0.92 excitons and 0.059 biexcitons, with smaller populations of triexcitons, etc. However, the partitioning in the last of the above coherent control studies was, as noted above, 0.606 excitons and 0.197 biexcitons. This is a significant deviation from the Poisson statistics and is achieved by saturating the exciton absorption. Similarly, in the coherent control scenario of Fig. 6, we find that 0.496 excitons and 0.257 biexcitons combine to provide an average exciton occupation of one exciton per QD, equal numbers of QDs containing one exciton and one biexciton can be realized at only $\approx1.25\times10^9$ W/cm^2. These are significant deviations from the Poisson-based results. Thus, the coherent control scenario enables us to overcome Poisson distribution requirements, providing a compelling new route by which gain thresholds may potentially be lowered in QD gain media.

V. CONCLUSION

We have shown, in a physically reasonable model, that the ratio of populations of biexcitons to excitons can be manipulated through an interference-based coherent control scenario. In addition to allowing for population control, the approach yields an all-optical control procedure to significantly reduce the optical gain threshold. In the case of CdSe quantum dots, the result is a reduction in the optical gain threshold by a factor of 50.

ACKNOWLEDGMENTS

The Natural Sciences and Engineering Research Council of Canada are gratefully acknowledged for support of this research. G.D.S. thanks the Alfred P. Sloan Foundation.

*Present address: Canadian Coast Guard College, Sydney, N.S. Canada.

[1] D. Bimberg, M. Grundmann, and N. N. Ledentsov, *Quantum Dot Heterostructures* (Wiley, Chichester, 1999).

[2] Al. L. Efros and A. L. Efros, Sov. Phys. Semicond. **16**, 772 (1982).

[3] L. E. Brus, J. Chem. Phys. **80**, 4403 (1984).

[4] S. V. Gaponenko, *Optical Properties of Semiconductor Nanocrystals* (Cambridge University Press, Cambridge, 1998).

[5] L. Bányai and S. W. Koch, *Semiconductor Quantum Dots* (World Scientific, Singapore, 1993).

[6] A. P. Alivisatos, J. Phys. Chem. **100**, 13226 (1996).

[7] C. Burda, X. B. Chen, R. Narayanan, and M. A. El-Sayed, Chem. Rev. **105**, 1025 (2005).

[8] V. I. Klimov, A. A. Mikhailovsky, S. Xu, A. Malko, J. A. Hollingsworth, C. A. Leatherdale, H.-J. Eisler, and M. G. Bawendi, Science **290**, 314 (2000); A. A. Mikhailovsky, S. Xu, A. Malko, J. A. Hollingsworth, M. G. Bawendi, and V. I. Klimov, Appl. Phys. Lett. **80**, 2380 (2002); H.-J. Eisler, V. C. Sundar, M. G. Bawendi, M. Walsh, H. I. Smith, and V. Klimov, *ibid.* **80**, 4614 (2002); S. A. Ivanov, J. Nanda, A. Piryatinski, M. Achermann, L. P. Balet, I. V. Bezel, P. O. Anikeeva, S. Tretiak, and V. I. Klimov, J. Phys. Chem. B **108**, 10625 (2004); M. Achermann, M. A. Petruska, S. Kos, D. L. Smith, D. D. Koleske, and V. I. Klimov, Nature (London) **429**, 642 (2004).

[9] C. E. Finlayson, D. M. Russell, C. M. Ramsdale, D. S. Ginger, C. Silva, and N. C. Greenham, Adv. Funct. Mater. **12**, 537 (2002).

[10] S. I. Shopova, G. Farca, A. T. Rosenburger, W. M. S. Wickramanayake, and N. A. Kotov, Appl. Phys. Lett. **85**, 6101 (2004).

[11] Y. Chan, J.-M. Caruge, P. T. Snee, and M. G. Bawendi, Appl. Phys. Lett. **85**, 2460 (2004).

[12] V. Sukhovatkin, S. Musikhin, I. Gorelikov, S. Cauchi, L. Bakueva, E. Kumacheva, and E. H. Sargent, Opt. Lett. **30**, 171 (2005).

[13] R. R. Cooney, S. L. Sewall, D. M. Sagar, and P. Kambhampati, Phys. Rev. Lett. **102**, 127404 (2009).

[14] M. Shapiro and P. Brumer, *Principles of the Quantum Control of Molecular Processes* (Wiley, New York, 2003).

[15] L.-A. Wu, A. Bharioke, and P. Brumer, J. Chem. Phys. **129**, 041105 (2008).

[16] J. Gong and P. Brumer, J. Chem. Phys. **132**, 054306 (2010).

[17] Z. Chen, P. Brumer, and M. Shapiro, J. Chem. Phys. **98**, 6843 (1993); Chem. Phys. Lett. **198**, 498 (1992).

[18] For a recent two-photon vs two-photon experimental result in atoms see M. C. Stowe, A. Pe'er, and J. Ye, Phys. Rev. Lett. **100**, 203001 (2008).

[19] Al. L. Efros, Phys. Rev. B **46**, 7448 (1992).

[20] J.-B. Xia, Phys. Rev. B **40**, 8500 (1989).

[21] Al. L. Efros, M. Rosen, M. Kuno, M. Nirmal, D. J. Norris, and M. Bawendi, Phys. Rev. B **54**, 4843 (1996); M. Nirmal, D. J. Norris, M. Kuno, M. G. Bawendi, Al. L. Efros, and M. Rosen, Phys. Rev. Lett. **75**, 3728 (1995).

[22] U. Woggon, F. Gindele, O. Wind, and C. Klingshirn, Phys. Rev. B **54**, 1506 (1996).

[23] M. Bayer, G. Ortner, O. Stern, A. Kuther, A. A. Gorbunov, A. Forchel, P. Hawrylak, S. Fafard, K. Hinzer, T. L. Reinecke, S. N. Walck, J. P. Reithmaier, F. Klopf, and F. Schäfer, Phys. Rev. B **65**, 195315 (2002).

[24] A. Franceschetti, L. Wang, H. Fu, and A. Zunger, Phys. Rev. B **58**, R13367 (1998); A. Franceschetti and A. Zunger, Phys. Rev. Lett. **78**, 915 (1997).

[25] T. Takagahara, Phys. Rev. B **62**, 16840 (2000); **47**, 4569 (1993).

[26] E. L. Ivchenko, Phys. Status Solidi A **164**, 487 (1997); S. V. Gupalov and E. L. Ivchenko, Phys. Solid State **42**, 2030 (2000); J. Cryst. Growth **184–185**, 393 (1998).

[27] A. S. Bracker, E. A. Stinaff, D. Gammon, M. E. Ware, J. G. Tischler, A. Shabaev, A. L. Efros, D. Park, D. Gershoni, V. L. Korenev, and I. A. Merkulov, Phys. Rev. Lett. **94**, 047402 (2005).

[28] M. Paillard, X. Marie, P. Renucci, T. Amand, A. Jbeli, and J. M. Gérard, Phys. Rev. Lett. **86**, 1634 (2001).

[29] T. Watanuki, S. Adachi, H. Sasakura, and S. Muto, Appl. Phys. Lett. **86**, 063114 (2005).

[30] O. I. Mićić, H. M. Cheong, H. Fu, A. Zunger, J. R. Sprague, A. Mascarenhas, and A. J. Nozik, J. Phys. Chem. B **101**, 4904 (1997).

[31] H. Htoon, P. J. Cox, and V. I. Klimov, Phys. Rev. Lett. **93**, 187402 (2004); H. Htoon, S. A. Crooker, M. Furis, S. Jeong, Al. L. Efros, and V. I. Klimov, *ibid.* **102**, 017402 (2009).

[32] J. Kim, C. Y. Wong, and G. D. Scholes, Acc. Chem. Res. **42**, 1037 (2009).

[33] M. R. Salvador, P. S. Nair, M. Cho, and G. D. Scholes, Chem. Phys. **350**, 56 (2008).

[34] S. L. Sewall, A. Franceschetti, R. R. Cooney, A. Zunger, and P. Kambhampati, Phys. Rev. B **80**, 081310(R) (2009).

[35] See, e.g., D. Gerbasi, M. Shapiro, and P. Brumer, J. Chem. Phys. **124**, 074315 (2006).

[36] A. R. Edmonds, *Angular Momentum in Quantum Mechanics*, 2nd ed. (Princeton University Press, Princeton, 1960).

[37] The transition dipole moment of CdSe quantum dots is not precisely characterized. A value of 7.6 D is reported for CdSe in photonic crystals in P. Lodahl, A. F. van Driel, I. S. Nikolaev, A. Irman, K. Overgaag, D. Vanmaekelbergh, and W. L. Vos, Nature (London) **430**, 654 (2004). We utilize a conservative value of 2 D, noting that the results in this paper are easily corrected for future changes in the value of the dipole. Specifically, the field amplitudes scale inversely to the value of the transition dipole.

[38] A. Corana, M. Marchesi, C. Martini, and S. Ridella, ACM Trans. Math. Softw. **13**, 262 (1987); W. L. Goffe, G. D. Ferrier, and J. Rogers, J. Econometr. **60**, 65 (1994); Fortran source code by W. L. Goffe.

[39] L. S. Li and A. P. Alivisatos, Adv. Mater. **15**, 408 (2003).